Crystallization of an amorphous lead zirconate titanate thin film with a dense-plasma-focus device

R. S. Rawat, M. P. Srivastava, S. Tandon, and A. Mansingh
Department of Physics and Astrophysics, University of Delhi, Delhi 110007, India
(Received 14 October 1992)

The pulsed ion beam of highly energetic argon ions that is generated during the focus phase of the dense-plasma-focus (DPF) device is used to crystallize the as-grown rf-sputtered amorphous thin film of lead zirconate titanate (PZT). Many samples of PZT thin films of different thicknesses are exposed to the DPF device. The 0.9-μm-thick PZT thin film is crystallized to the desired rhombohedral phase. The scanning electron microscopy photograph of this film indicates a reasonably good surface quality.

INTRODUCTION

The dense-plasma-focus (DPF) (Refs. 1–3) device is a simple and easily accessible device that makes use of a self-generated magnetic field for compressing the plasma to very high densities ($\simeq 10^{25}$–10^{26} m^{-3}) and high temperatures ($\simeq 1$–2 keV). The DPF has been established as a source of fusion neutrons (having flux in the range of 10^{8}–10^{12} neutrons per burst), x rays, energetic ions,[4–6] and electrons[7–9] with energies of several hundred keV and above. Being a source of such a wide range of phenomena, the DPF has been successfully applied as a neutron source for pulsed activation analysis,[10] as a spectroscopic source for the production of highly ionized species,[11] as a pump source for lasers,[12] and as a high-flux soft-x-ray source for x-ray lithography.[13] Besides this, it has been recognized as a possible magnetic fusion device with potential applications such as a neutron source of high fluence for blanket studies for controlled thermonuclear reactor and material problems,[14] as a nuclear design test facility,[15] as the nuclear core of a hybrid fusion-fission system,[15] as a driver in the inertial confinement fusion,[16] etc.

It is well known that the crystalline lead zirconate titanate (PZT) thin film has a wide range of applications[17] in thin-film devices such as ferroelectric memories,[18] piezoelectric transducers, electro-optic displays,[19] and pyroelectric sensors.[20] The as-grown PZT thin film, deposited on room-temperature substrates by rf sputtering, is amorphous in nature. Various techniques such as post deposition annealing[21] and rapid thermal annealing[22] have been reported for crystallization of amorphous PZT films. Keeping in mind the importance of crystalline PZT thin films, we have used DPF as a plasma processor to induce crystallization in as-grown rf-sputtered amorphous thin films of PZT as reported in this paper. The relative merits of various techniques for crystallization are yet to be established.

We have exposed as-grown rf-sputtered amorphous PZT thin films of different thicknesses to DPF shots at different distances from the top of the anode. The exposed thin films were analyzed using an x-ray diffractometer and scanning electron microscope to investigate the changes in the nature and surface morphology of the films.

EXPERIMENTAL ARRANGEMENT AND METHODOLOGY

The DPF device at our Plasma Research Laboratory is as shown in Fig. 1. It is a Mather-type focus with 3.3 kJ of energy which is being energized by a single 30-μF, 15-kV fast discharging energy storage capacitor. The other subsystems of DPF are (1) the focus chamber, a chromed mild steel cylindrical chamber consisting of coaxial assembly of electrodes with one hollow anode being surrounded by six symmetrically placed cathodes around it; (2) the high voltage charger, to charge the capacitor to a value of 14 kV which is slightly lower than the maximum rating of the capacitor; (3) the spark gap, to transmit the high voltage from the capacitor to the electrodes inside the focus chamber; and (4) the triggering electronics, to activate the spark gap switch.

The capacitor is charged by the high voltage charger and then the spark gap is triggered to transfer the energy from the capacitor to the focus chamber. The gas breakdown occurs initially across the surface of the insulator,

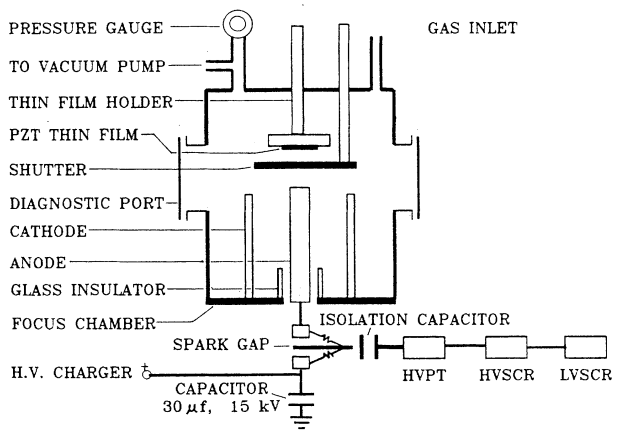

FIG. 1. Experimental setup of dense-plasma focus for crystallization of PZT thin films.

separating the anode and cathode. The resultant current sheath is accelerated axially up the chamber by the $j_r B_\theta$ force (j_r being radial current density and B_θ the azimuthal magnetic field) in the axial acceleration phase. Upon reaching the top of the anode the current sheath collapses radially inward due to the $j_z B_\theta$ force (j_z being axial current density) during the focus phase of DPF. The onset of $m=0$ instability during focus phase enhances the induced electric field locally. This enhanced electric field together with the magnetic field accelerates more electrons toward the inner electrode (anode) and ions in the opposite direction towards the top of the DPF chamber. We have utilized this pulsed ion beam of highly energetic ions for irradiating amorphous thin films of PZT.

Argon ion beam emitted in DPF has a pulse length of about 8–10 ns (full width at half maximum) with ions having energies in the range of 25 keV to about 8 MeV. The average ion energy is about 300–400 keV. The pulse shape is nearly Gaussian. The total number of fast ions outside the focus pinch is about 10^{17}. According to one of the estimates,[9] the energy associated with the ion beam is about 8% of the total energy of the capacitor bank. Therefore, the total energy of the pulsed ion beam in our case is about 240 J. The energy density of the ion beam on the sample placed at a distance of 4.2 cm is about 1.2×10^6 J/m^2. The energy density of the ion beam on the sample changes with the variation of the distance of the sample from the top of the anode. The percentage of impurities is about 1% which includes Cu ions and impurities in various ionization states, such as O^+-O^{8+}, N^+-N^{7+}, and C^+-C^{6+} ions.

The films were prepared using a NORDIKO 2000 rf sputtering system. The films were sputtered from a 4-in. oxide target of $Pb(Zr_{0.53}Ti_{0.47})O_3$ material having 12% excess PbO. The excess PbO was added in the target because it is well known that a loss of Pb in rf-sputtered films occurs due to resputtering of Pb. The system was pumped down to a pressure of 6.5×10^{-5} Pa before argon gas was introduced into the system and thereafter maintained at a pressure of 0.92 Pa. The plasma is struck inside the vacuum chamber under the rf field (at the rf power of 200 W) and a self-bias of 1.3 kV was generated. The films were grown on glass substrates at room temperature and the target to substrate distance was 10 cm. The as-grown films were amorphous [Figs. 2(a) and 3(a)].

The samples (films on the glass substrate) were mounted axially above the anode as shown in Fig. 1. The energetic ion beam from the focus region was allowed to strike the sample which was attached to the axially movable brass mount. This energetic ion beam is produced when focusing is good and it was achieved after a few shots at the optimum argon pressure (80 Pa). The expo-

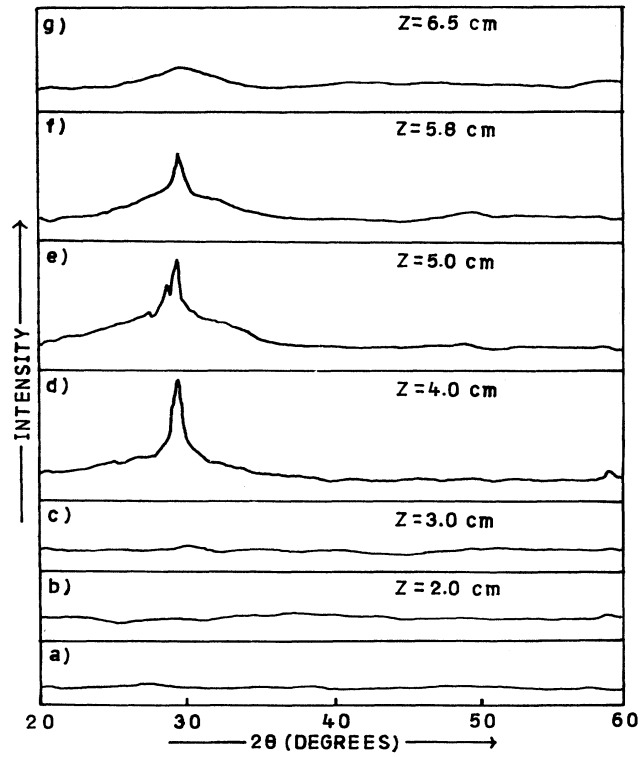

FIG. 2. XRD patterns of sample I: (a) unexposed to plasma shots and (b)–(g) exposed by a single DPF shot at different distances Z from the anode. Pressure of argon = 80 Pa.

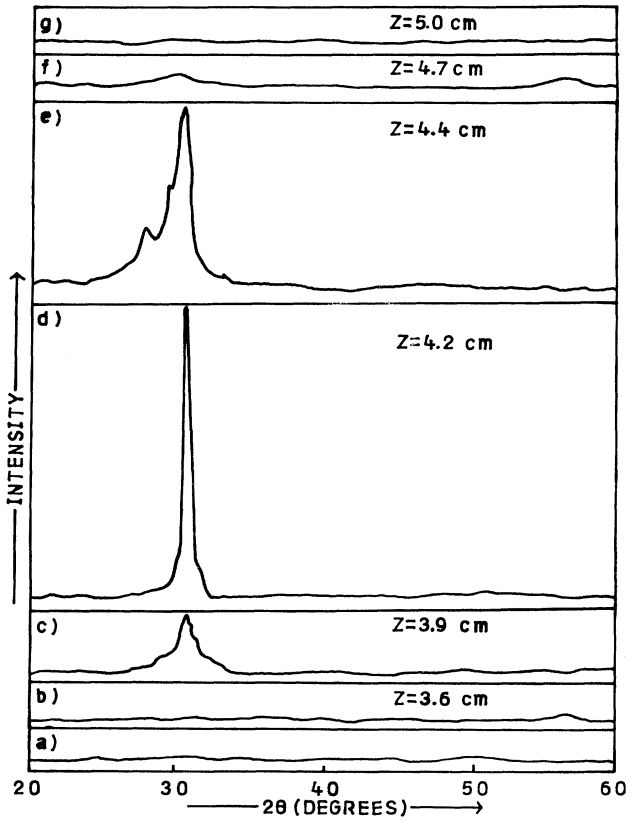

FIG. 3. XRD patterns of sample II: (a) unexposed to plasma shots, and (b)–(g) exposed by a single DPF shot at different distances Z from the anode. Pressure of argon = 80 Pa.

sure of the samples to the weak ion beam (produced while optimizing the DPF for good focusing) was avoided by using an aluminum shutter arrangement in between the anode and the sample as shown in Fig. 1. The aluminum shutter was removed when proper focusing was obtained and thereby exposing the sample to energetic ion beam. Lee *et al.*[23] have shown that any obstacle placed above the anode will not affect the plasma focus dynamics and focusing action if its distance from the top of the anode is greater than the anode radius. Hence we always placed the sample at a distance greater than 1 cm, which is the anode radius. Argon was used as the gaseous medium inside the focus chamber. The charging voltage of the capacitor was always 14 kV.

RESULTS AND DISCUSSION

We have taken two PZT thin films one of thickness 0.4 μm (sample I) and the other of thickness 0.9 μm (sample II). The samples after the exposure to DPF shots have been analyzed utilizing a Phillips PW 1840 diffractometer and a JEOL JSM-840 scanning electron microscope.

The experiment was initially performed with sample I. The unexposed sample was amorphous as shown by an x-ray-diffraction (XRD) pattern in Fig. 2(a). The samples were kept at different distances Z from the top of the anode. When exposed at $Z=1.5$ cm, visual observation showed that the film was removed and the glass substrate cracked. For distances $Z=2.0$ and 3.0 cm the substrate was not damaged but the film was removed. No crystallization was induced in the glass substrate, as the XRD patterns did not show any peak [Figs. 2(b) and 2(c)]. Figure 2(d) shows that when the sample was placed at $Z=4.0$ cm fairly good crystallization occurs. The samples exposed at $Z=5.0$ and 5.8 cm have XRD patterns as shown in Figs. 2(e) and 2(f). The degree of crystallization was found to decrease which finally disappeared at $Z=6.5$ cm [Fig. 2(g)]. The main peak at the angle $2\theta=29.4°$ suggests the pyrochloral phase. This phase appears when there is a deficiency of Pb in the sample. The film is polycrystalline with the grain size varying from a meager 130 Å for Fig. 2(f) to as large as 304.35 Å for the thin film exposed at $Z=4.0$ cm [Fig. 2(d)].

The unexposed film of sample II was amorphous as shown in Fig. 3(a). The XRD patterns of the sample II, exposed to a single shot at different distances Z are shown in Figs. 3(b)–3(g). The XRD pattern as shown in Fig. 3(d) shows a sharp peak depicting the good amount of crystallization. This corresponds to the sample being exposed at the distance $Z=4.2$ cm. The amount of crystallization as inferred from the peaks of the XRD patterns, has been found to increase when Z is changed from 3.6 to 4.2 cm [Figs. 3(b)–3(d)]. The crystallization decreases as we further increase Z up to 4.7 cm [Figs. 3(e) and 3(f)] and finally disappears at $Z=5.0$ cm [Fig. 3(g)]. The main peak at the angle $2\theta=30.7°$ indicates the rhombohedral phase and suggests that the lead loss in 0.9-μm-thick films is not as much as in 0.4-μm-thick films. The grain sizes for polycrystalline films corresponding to Figs. 3(c), 3(d), and 3(e) are 203.1, 304.6, and 166.4 Å, respectively.

Since the thin film of sample II did not show any crystallinity at $Z=5.0$ cm, we investigated to see if two shots can bring about crystallinity. Figure 4 shows the XRD pattern of sample II placed at the distance $Z=5.0$ cm with two DPF shots. It is observed that the crystallinity can be induced to a reasonable degree.

In order to see if focusing is important to crystallize the thin film, we have also exposed sample I to the single DPF shot at different pressures of argon gas, viz., 20, 80, 1.5×10^2, and 2.2×10^2 Pa. The samples were kept at $Z=4.0$ cm since at this distance the sample showed the good crystallinity with an argon pressure of 80 Pa. The XRD patterns of all these exposures are as shown in Figs. 5(a)–5(d). We found that crystallinity was absent in all the exposures at pressures other than 80 Pa. The corresponding voltage signals of DPF discharges at pressures other than 80 Pa on oscilloscope showed improper focusing. This suggests that the focusing phase, which causes the generation of intense and energetic ion beams, is necessary to induce crystallization in the thin film of PZT.

The surface morphology of the exposed samples that exhibit good crystallinity is studied by scanning electron microscopy (SEM). Figures 6 and 7 show the micrographs of sample I, exposed at $Z=4.0$ cm, and of sample II, exposed at $Z=4.2$ cm, respectively. Both micrographs show that the surface is not smooth and has craters and pit holes on them. The SEM photo of 0.4-μm-thick thin films (Fig. 6) shows large grains with many pit holes on the film surface indicating poor surface quality of PZT film. However, the 0.9-μm film shows (Fig. 7) crystalline character with small microcrystals surrounding the big grains. The pit holes indicated by black spots are almost negligible. The overall surface quality of crystallized 0.9-μm films is reasonably good and is comparable to the one reported by Dana, Etzold, and Clabes.[24] The micrograph in Fig. 7 also suggests that the Hillock formation has taken place on 0.9-μm-thick PZT thin films of sample II. The phase transformation is being induced by bombarding argon ions which impart energy

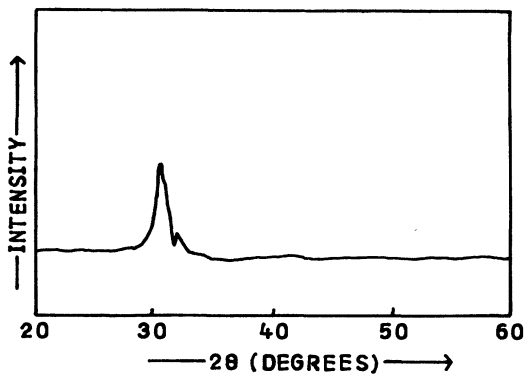

FIG. 4. XRD pattern of sample II exposed to two DPF shots at $Z=5.0$ cm. Pressure of argon = 80 Pa.

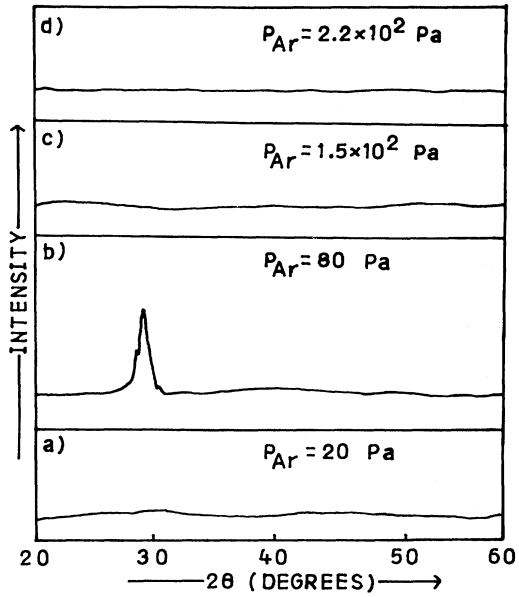

FIG. 5. XRD patterns of sample I placed at $Z=4.0$ cm and exposed to a single DPF shot at different argon pressure.

and stress on the thin-film surface. The large craters on the film surface presumably is to relieve this stress.

In order to do the TEM study the thickness of the film should be about 0.1 μm, but with this thickness crystallization of the film was not achieved on being exposed to DPF shots at different distances from the top of the anode. This may be due to excessive Pb loss from this very thin film. Consequently, it was not possible to perform the TEM studies.

The as-grown films of different thicknesses had the same composition since they were deposited under identical sputtering conditions. It is well known that Pb plays an important role in the crystallization of PZT films. Highly Pb deficient films do not crystallize, slightly Pb deficient films crystallize to the pyrochloral phase,

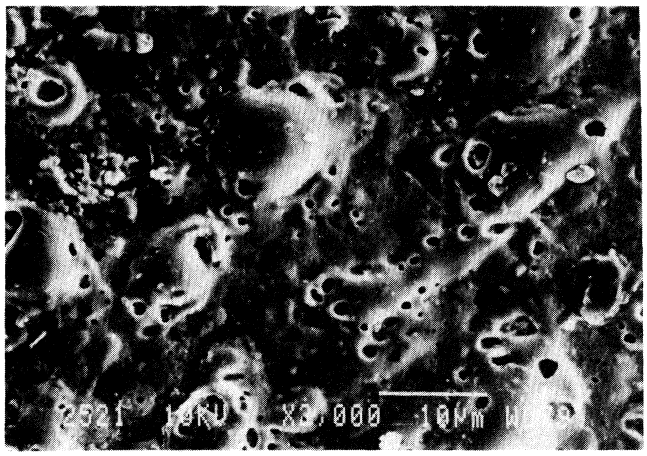

FIG. 6. SEM of sample I exposed at $Z=4.0$ cm.

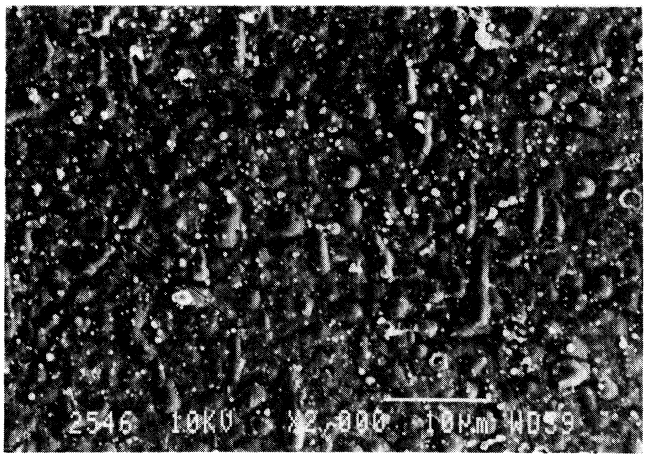

FIG. 7. SEM of sample II exposed at $Z=4.2$ cm.

whereas films with optimum Pb content crystallize to the pervoskite (rhombohedral) phase. Since 0.1 μm films do not crystallize, whereas 0.4- and 0.9-μm films crystallize to pyrochloral [Figs. 2(d)–2(f)] and pervoskite phases [Figs. 3(b)–3(f)], respectively, this suggests that the percentage Pb loss during exposure to DPF is different for films of different thicknesses. The process involved appears to be a liquid-phase process and can be understood in the following manner. Short ion pulses having high-energy density can cause very rapid heating of the surface region,[25] especially for insulators of low thermal conductivity such as PZT. The rise in surface temperature results in the melting of the film near the surface. High Pb loss from a melted PZT portion will occur because it is more volatile. The heat and melt front produced at the film surface propagates towards film-substrate interface.[26] The melt depth and the duration of the liquid phase of surfaces depend on the power of incident ion beams. The thickness of the molten region will be independent of the thickness of the films. Hence, the percentage of Pb loss from the entire volume will be less for thicker films. The melting may be confined to a small region near the surface but the temperature of the entire film may be high enough to create a liquidlike disordered state. The high temperature also causes the Pb diffusion from Pb rich to Pb deficient regions giving a homogeneous film with the area of about 1 cm^2. The melted region then resolidifies and depending on the percentage of Pb loss from the film, the film goes to amorphous (0.1-μm film), pyrochloral (0.4-μm film), and pervoskite (0.9-μm film) phases as is observed.

It may be further noted from Figs. 2 and 3 that the crystallinity can be brought to the amorphous thin film of PZT when they are exposed to the DPF discharges at an optimum distance in the range of $Z=4.0$–4.4 cm at the pressure of argon suitably adjusted so that proper focusing can take place. Conversion of amorphous samples to crystalline structure at a particular distance from the top of the anode leads one to conclude that the ion beam with the specific energy density is required to bring about such

changes. The 0.9-μm-thick PZT thin film has been crystallized to the rhombohedral phase and its reasonably good surface quality indicates that one can achieve a crystalline ferroelectric PZT thin film by DPF processing of as-grown amorphous thin film.

ACKNOWLEDGMENTS

R. S. R. is grateful to the Council of Scientific and Industrial research, India and S. T. is grateful to the University Grant Comission, India for financial support.

[1]J. W. Mather, Phys. Fluids **7**, 5 (1964).

[2]N. V. Filippov, T. I. Filippova, and V. P. Vinogradov, Nucl. Fus. **2**, 577 (1962).

[3]S. Lee, T. Y. Tou, S. P. Moo, M. A. Eissa, A. V. Gholap, K. H. Kwek, S. Mulyodrono, A. J. Smith, Suryadi, W. Usada, and M. Zakaullah, Am. J. Phys. **56**, 62 (1988).

[4]R. L. Gullickson and H. L. Sahlin, J. Appl. Phys. **49**, 1099 (1978).

[5]G. Gerdin, W. Stygar, and F. Venneri, J. Appl. Phys. **52**, 3269 (1981).

[6]U. Jager and H. Herold, Nucl. Fus. **27**, 407 (1987).

[7]K. Schmitt, H. Krompholz, F. Ruhl, and G. Herziger, Phys. Lett. **95A**, 239 (1975).

[8]W. L. Harries, J. H. Lee, and D. R. McFarland, Plasma Phys. **20**, 95 (1978).

[9]W. Stygar, G. Gerdin, F. Venneri, and J. Mandrekas, Nucl. Fus. **22**, 1161 (1982).

[10]E. Bar Auraham and Y. Porath, Nucl. Instrum. Methods **123**, 5 (1975).

[11]E. H. Beckner, J. Appl. Phys. **37**, 4944 (1966).

[12]N. P. Kozlov, V. A. Alekseev, Yu. S. Protasov, and A. N. Rubinov, Pis'ma Zh. Eksp. Teor. Fiz. **20**, 716 (1974) [JETP Lett. **20**, 331 (1974)].

[13]Y. Kato and S. H. Be, Appl. Phys. Lett. **48**, 686 (1986).

[14]P. Cloth and H. Conard, Nucl. Sci. Eng. **62**, 591 (1977).

[15]J. P. Rager, in *Unconventional Approach to Fusion,* edited by B. Brunelli and G. Leotta (Plenum, New York, 1982).

[16]R. Gratton, A. R. Piriz, and J. O. Pouzo, Nucl. Fus. **26**, 483 (1986).

[17]A. Mansingh, Ferroelectrics (UK) **102**, 69 (1990).

[18]C. A. Aaz De Araujo, L. D. McMillan, B. M. Melnick, J. D. Cuchiaro, and J. F. Scott, Ferroelectrics (UK) **104**, 241 (1990).

[19]H. Adaci, T. Mitsaya, D. Yamazaki, and K. Wasa, J. Appl. Phys. **60**, 736 (1986).

[20]R. Takayama, T. Yomita, K. Tijima, and I. Veda, J. Appl. Phys. **61**, 411 (1987).

[21]K. Sreenivas and M. Sayer, J. Appl. Phys. **64**, 1484 (1988).

[22]C. V. R. Vasant Kumar, M. Sayer, R. Pascual, D. T. Amm, and D. M. Swanston, Appl. Phys. Lett. **58**, 1161 (1991).

[23]S. Lee, M. A. Alabraba, A. V. Gholap, S. Kumar, K. H. Kwek, M. Nisar, R. S. Rawat, and J. Singh, IEEE Trans. Plasma Sci. **18**, 1028 (1990).

[24]S. S. Dana, K. F. Etzold, and J. Clabes, J. Appl. Phys. **8**, 4398 (1991).

[25]J. E. E Baglin, R. T. Hodgson, W. K. Chu, J. M. Neri, D. A. Hammer, and L. J. Chen, Nucl. Instrum. Methods **191**, 169 (1981).

[26]T. Brat, M. Eizenberg, R. Fastow, C. J. Palmstrom, and J. W. Mayer, J. Appl. Phys. **57**, 264 (1985).

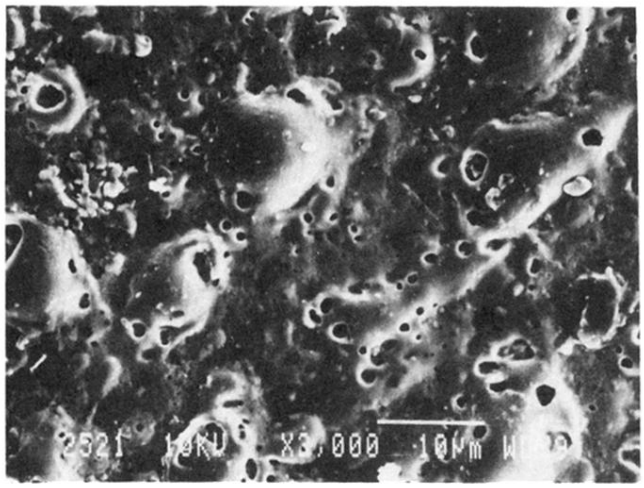

FIG. 6. SEM of sample I exposed at $Z = 4.0$ cm.

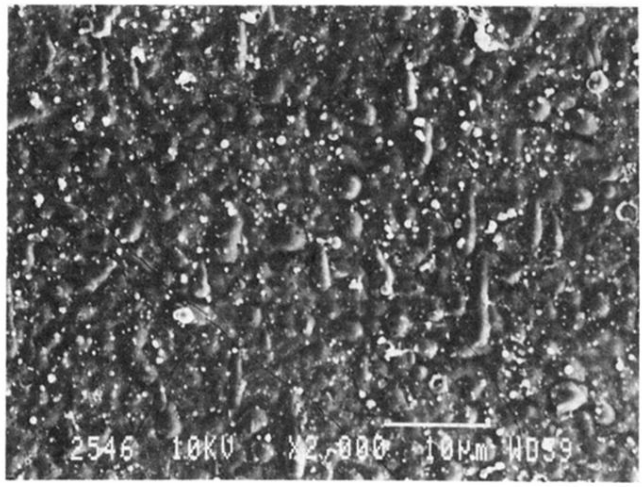

FIG. 7. SEM of sample II exposed at $Z=4.2$ cm.